Journal of Photochemistry & Photobiology A: Chemistry 397 (2020) 112598

Contents lists available at ScienceDirect

Journal of Photochemistry & Photobiology A: Chemistry

journal homepage: www.elsevier.com/locate/jphotochem

Non-cytotoxic photostable monomethine cyanine platforms: Combined paradigm of nucleic acid staining and *in vivo* imaging

Atanas Kurutos[a,*], Tatjana Ilic-Tomic[b], Fadhil S. Kamounah[c], Aleksey A. Vasilev[d], Jasmina Nikodinovic-Runic[b,*]

[a] Institute of Organic Chemistry with Centre of Phytochemistry, Bulgarian Academy of Sciences, Acad. G. Bonchev str., bl. 9, 1113 Sofia, Bulgaria
[b] Institute of Molecular Genetics and Genetic Engineering, University of Belgrade, Vojvode Stepe 444a, 11000 Belgrade, Serbia
[c] University of Copenhagen, Department of Chemistry, Universitetsparken 5, DK-2100 Copenhagen, Denmark
[d] Department of Pharmaceutical and Applied Organic Chemistry, Faculty of Chemistry and Pharmacy, Sofia University, 1164 Sofia, Bulgaria

ARTICLE INFO

Keywords:
Cyanine dyes
Fluorescent microscopy
Microbial cell staining
Nucleic acid detection
Non-Cytotoxic molecular probes

ABSTRACT

Cyanine based chemosensing platforms have successfully been employed over the past couple of decades in various fields of biomolecular sciences. Still a substantial number of recent advances and improvements on this class of compounds are reported in the art. This paper presents our latest work on the improved synthetic approach, study on photophysical properties, and biosensing applicability of monomethine cyanine dyes. The series of mono-, di- and tricationic dyes showed up to 5-fold enhanced resistance against photobleaching compared to the commercially available Thiazole Orange (TO). The title compounds were studied as potential molecular probes for the detection of deoxyribonucleic acid, demonstrating their capacity as excellent fluorescent labeling agents. Depending on the dye chemical structure, current Cl-TO compounds exhibit up to 834-fold enhanced fluorescence emission and form stable complexes with *Calf Thymus*-DNA. The calculated binding constants were found to be higher than several conventional fluorogenic dyes for nucleic acid detection. All studied derivatives appeared as less cytotoxic than the Thiazole Orange. IC50 concentrations in human fibroblasts MRC5 cell line were calculated up to 50 μM for the synthesized Cl-TO dyes, and 0.5 μM for the parental Thiazole Orange. Two of the dyes were found very competent in post-electrophoretic visualization of DNA. As demonstrated by the agarose gel electrophoresis, the staining efficiency and detection limits of the dyes were comparable to the widely used Ethidium Bromide. The tricationic dye revealed great potential for cell cycle analysis in G1, S and G2 phases. The chlorinated TO derivatives readily stain human cells *in vivo*, while they can effectively be applied for eukaryotic and microbial cell staining.

1. Introduction

Due to their excellent photophysical properties and great biocompatibility, the group of cyanine dyes has undeniably acquired the popularity of a robust chemosensing platform for the visualization of various biologically important processes. Biomolecular imaging technologies including fluorescent labelling [1–5], tumour cell line markers [6–8], super-resolution imaging [9], enzymatic and immune-assays [10], nucleic acid sequencing [11,12], purification and sizing of deoxyribonucleic acid fragments [13], optical sensing [14,15], detection of proteins [16], interactions with lipids [17], detection of reactive oxygen species [18], drug delivery [19], and theranostic [20,21] are only few examples on recent advances and topics of this class of organic compounds.

Among numerous spectroscopic techniques, fluorescence-based methods are commonly employed for highly accurate detection of nucleic acids. Intrinsically non-emittive in aqueous media, cyanines acquire strong fluorescence response when forced immobilization of the dye backbone occurs within the target binding sites of DNA or RNA. This is due to loss of mobility around the methine bond joining the two heterocyclic chromophores [22]. The nonradiative coupled photoisomerization and the torsional motion between the benzothiazolium and the quinolinium moieties account for reported quantum yield as low as 0.0002 in aqueous solutions [23]. Over the past decade, the continuous and rapid development of new devices and instrumentarium for the detection of biologically important samples appealed to the design of specific labelling small molecules. High molar extinction coefficients, enhanced fluorescence emission response, resistance

* Corresponding authors.
E-mail addresses: akouroutos@gmail.com (A. Kurutos), jasmina.nikodinovic@imgge.bg.ac.rs (J. Nikodinovic-Runic).

https://doi.org/10.1016/j.jphotochem.2020.112598
Received 28 October 2019; Received in revised form 24 April 2020; Accepted 25 April 2020
Available online 05 May 2020
1010-6030/

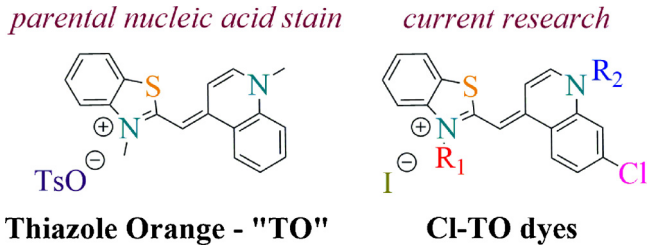

Fig. 1. Molecular representation of the parental nucleic acid stain "Thiazole Orange – TO" and current Cl-TO monomethine cyanine derivatives under study.

against photobleaching, negligible spectral overlap with target biomolecules, binding selectivity, strong complexation with DNA, and low cytotoxicity are key factors to the successful design of new fluorogenic probes.

Earlier, Shank and co-workers examined the effect of halogen atoms to the monomethine scaffold, where an increased brightness and photostabilizing effect were addressed [24]. Further reports also revealed advantages upon addition of a strong electron acceptor (*e.g.* a CF_3 group) to the quinolinium moiety [25]. Similarly, the introduction of a CN group to the cyanine backbone improves the photophysical properties and decreases the susceptibility of the chromophore towards singlet oxygen species [26]. The α-CN-TO dye proved to exhibit superior photostability and brightness, however it was found to be non-fluorescent in the presence of dsDNA. This modified cyanine was unsuitable for binding nucleic acids due to significantly twisted geometry. Previously, we also reported halogen-containing Thiazole Orange derivatives, whose optical properties were found promising for continuous investigation [27]. The aim of our extended study is to design a series with improved photophysical characteristics, good biocompatibility, and increased labelling capacity (Fig. 1).

To achieve our goal, current efforts were focused on: i) improve the synthetic protocol for the preparation of monomethine cyanine scaffold; ii) prepare TO analogues carrying single or multiple positive charges; iii) evaluate the photophysical characteristics in both organic media and buffer solutions; iv) study the resistance against photobleaching; v) examine the *in vivo* cytotoxicity; vi) apply the newly synthesized dyes to cell cycle analysis and last but not least vii) demonstrate bioimaging applications of current fluorogenic compounds.

2. Materials and methods

2.1. Analysis methods and equipment

All chemicals and solvents required for the synthesis of the dyes were purchased from Sigma-Aldrich, Alfa-Aesar, Acros Organics, Merck and used as received. The high-performance liquid chromatography (HPLC) grade solvents used for the spectroscopic analyses were purchased form Sigma-Aldrich, Scharlau Chemicals, and Macron Fine Chemicals TM. Deuterated solvents were purchased from Eurisotop and used as received. All other starting materials and solvents were commercial products of analytical grade. Purification of the target cyanines was achieved by repeated recrystallization from absolute ethanol. Analytical thin-layer chromatography (TLC) was performed on Merck silica gel 60 F254 0.2 mm-thick precoated TLC plates using chloroform : methanol : acetic acid (86:13:1 v/v) as a mobile phase. Spots were visualised under VILBER Ultraviolet Lamp BVL-6.LC Dual Wavelength 254/365 nm and power of 2 × 6 W. The identity of the compounds was confirmed by various spectroscopic techniques including NMR and mass spectrometry. ^{1}H-NMR and ^{13}C-NMR spectra were recorded using 5 mm tubes at 500.13 MHz and 125.77 MHz, respectively, in DMSO-d_6 at 25 °C on a Bruker Ultrashield Plus 500 spectrometer. The signals corresponding to the residual protons of DMSO-d_6 at 2.50 ppm were used as an internal reference. All chemical shifts (δ) are quoted in ppm with accuracy of 0.01 ppm. Coupling constants *J* are expressed in Hz and determined with accuracy of 0.1 Hz. The following abbreviations are quoted to describe spin multiplicity in ^{1}H-NMR: *ss* = singlet, d = doublet, t = triplet, q = quartet, *dd* = doublet of doublets, *ddd* = doublet of doublets of doublets, *m* = multiplet. HRMS LC/MS were recorded on a Dionex Acclaim RSLC 120 C18 2.2 μm 120 Å 2.1 × 50 mm column maintained at 40 °C carried out on a Bruker MicrOTOF-QII-system with ESI-source with nebulizer 1.2 bar, dry gas 8.0 L/min, dry temperature 200 °C, capillary 4500 V and plate offset -500 V.

2.2. Synthesis of intermediate products

Intermediates **2c**, **3a-3c**, **5d** and **6a-6d** were obtained by reported protocols [28–33].

2.3. Synthesis of the target Cl-TO monomethine cyanine dyes

A mixture of *N*-quaternary-2-methylbenzothiazolium salt **3a-3c** (1 mmol) and the corresponding 4,7-dichloroquinolinium derivative **6a-6d** (1 mmol) were suspended in ethanol / dichloromethane (15 mL, 3:2 v/v). An excess of *N,N*-diisopropylethylamine (2 equiv., 0.35 mL, 2 mmol) was added dropwise over 5 min, and the resulting mixture was vigorously stirred under argon atmosphere for 3 h at room temperature. A spontaneous advent of red colour was observed followed by the formation of thick precipitate (Scheme 1). The crude product was collected by filtration, washed with diethyl ether (3 × 20 mL) and dried under reduced pressure, affording the monomethine cyanine dyes as red solids. Repeated recrystallization from absolute ethanol yielded the analytical samples of the target Cl-TO dyes.

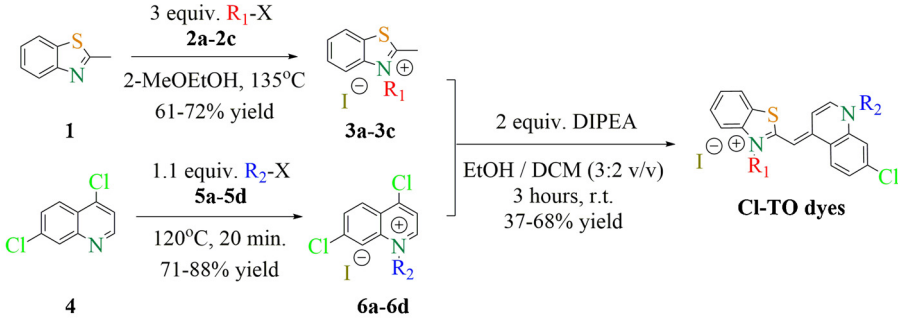

Cl-TO-1: R_1= CH_3 R_2 = CH_3 **Cl-TO-2**: R_1= C_4H_9 R_2 = CH_3 **Cl-TO-3**: R_1= C_4H_9 R_2 = C_2H_5

Cl-TO-4: R_1= C_4H_9 R_2 = $CH_2C_6H_5$ **Cl-TO-5**: R_1= $C_3H_6N^+C_5H_5$ Br^- ,R_2 = $CH_2C_6H_5$

Cl-TO-6: R_1= $C_3H_6N^+C_5H_5$ Br^- ,R_2 = $C_3H_6NC_5H_4N^+(CH_3)_2$ Br^-

Scheme 1. Improved synthetic approach to the fluorogenic Cl-TO monomethine cyanine dyes.

2-((7-chloro-1-methylquinolin-4(1 H)-ylidene)methyl)-3-methylbenzo[*d*]thiazol-3-ium iodide (**Cl-TO-1** (TO-7Cl / [27]) – (Figs. S1 − 3 / Supporting Information), red solid, yield = 45 %; ^{1}H-NMR (500 MHz, DMSO-d_6) δ 8.82 (d, J = 9.3 Hz, 1 H), 8.54 (d, J = 7.2 Hz, 1 H), 8.13 (d, J = 2.1 Hz, 1 H), 8.06 (dd, J = 8.0, 1.2 Hz, 1 H), 7.80 (d, J = 8.3 Hz, 1 H), 7.78 (dd, J = 9.1, 2.1 Hz, 1 H), 7.63 (ddd, J = 8.5, 7.3, 1.2 Hz, 1 H), 7.46 – 7.41 (m, 1 H), 7.32 (d, J = 7.2 Hz, 1 H), 6.91 (s, 1 H), 4.12 (s, 3 H), 4.03 (s, 3 H); ^{13}C-NMR (126 MHz, DMSO-d_6) δ 160.51, 148.01, 145.37, 140.44, 138.98, 138.03, 128.25, 127.65, 126.89, 124.71, 124.00, 122.93, 122.68, 117.78, 113.20, 107.79, 88.40, 42.40, 33.98; HR ESP MS: *m/z*: Found 339.07457 [M+] $C_{19}H_{16}ClN_2S^+$; Requires [M+] 339.0717;

3-butyl-2-((7-chloro-1-methylquinolin-4(1 *H*)-ylidene)methyl) benzo[*d*]thiazol-3-ium iodide (**Cl-TO-2**) – (Figs. S4 − 6 / Supporting Information), red solid, yield = 61 %; ^{1}H-NMR (500 MHz, DMSO-d_6) δ 8.82 (d, J = 9.3 Hz, 1 H), 8.54 (d, J = 7.2 Hz, 1 H), 8.13 (d, J = 2.1 Hz, 1 H), 8.07 (dd, J = 8.0, 1.2 Hz, 1 H), 7.81 − 7.78 (m, 2 H), 7.63 (ddd, J = 8.5, 7.3, 1.2 Hz, 1 H), 7.46 – 7.43 (m, 1 H), 7.36 (d, J = 7.2 Hz, 1 H), 6.92 (s, 1 H), 4.66 (t, J = 7.4 Hz, 2 H), 4.13 (s, 3 H), 1.80 − 1.74 (dq, J = 9.9, 7.4 Hz, 2 H), 1.49 − 1.42 (m, 2 H), 0.93 (t, J = 7.4 Hz, 3 H); ^{13}C-NMR (126 MHz, DMSO-d_6) δ 160.51, 148.01, 145.37, 140.44, 138.98, 138.03, 128.25, 127.65, 126.89, 124.71, 124.00, 122.93, 122.68, 117.78, 113.20, 107.79, 88.40, 42.40, 33.98.; HR ESP MS: *m/z*: Found 381.11886 [M+] $C_{22}H_{22}ClN_2S^+$; Requires [M+] 381.1187;

3-butyl-2-((7-chloro-1-ethylquinolin-4(1 H) ylidene)methyl)benzo [*d*]thiazol-3-ium iodide (**Cl-TO-3**) – (Figs. S7 − 9 / Supporting Information), red solid, yield = 52 %; ^{1}H-NMR (500 MHz, DMSO-d_6) δ 8.76 (d, J = 9.2 Hz, 1 H), 8.59 (d, J = 7.3 Hz, 1 H), 8.22 (d, J = 2.1 Hz, 1 H), 8.07 (dd, J = 7.9, 1.2 Hz, 1 H), 7.81 (d, J = 8.3 Hz, 1 H), 7.77 (dd, J = 9.0, 2.0 Hz, 1 H), 7.62 (ddd, J = 8.4, 7.2, 1.2 Hz, 1 H), 7.47 – 7.41 (m, 1 H), 7.36 (d, J = 7.3 Hz, 1 H), 6.91 (s, 1 H), 4.66 (t, J = 7.3 Hz, 2 H), 4.61 (q, J = 7.2 Hz, 2 H), 1.84 – 1.70 (m, 2 H), 1.44 (t, J = 7.2 Hz, 5 H), 0.93 (t, J = 7.3 Hz, 3 H); ^{13}C-NMR (126 MHz, DMSO-d_6) δ 160.11, 148.08, 144.26, 139.92, 138.31, 137.81, 128.34, 127.88, 126.97, 124.80, 124.08, 123.03, 122.91, 117.28, 113.32, 108.25, 88.15, 49.37, 45.71, 29.28, 19.41, 14.63, 13.79; HR ESP MS: *m/z*: Found 395.13447 [M+] $C_{23}H_{24}ClN_2S^+$; Requires [M+] 395.1343;

2-((1-benzyl-7-chloroquinolin-4(1 *H*)-ylidene)methyl)-3-butylbenzo [*d*]thiazol-3-ium iodide (**Cl-TO-4**) – (Figs. S10 − 12 / Supporting Information), red solid, yield = 68 %; ^{1}H-NMR (500 MHz, DMSO-d_6) δ 8.78 (d, J = 9.3 Hz, 1 H), 8.71 (d, J = 7.4 Hz, 1 H), 8.12 (dd, J = 8.0, 1.2 Hz, 1 H), 8.04 (d, J = 2.1 Hz, 1 H), 7.87 (d, J = 8.4 Hz, 1 H), 7.72 (dd, J = 9.1, 2.0 Hz, 1 H), 7.66 (ddd, J = 8.5, 7.3, 1.2 Hz, 1 H), 7.54 – 7.46 (m, 1 H), 7.45 (d, J = 7.3 Hz, 1 H), 7.40 (tt, J = 8.0, 1.5 Hz, 2 H), 7.37 – 7.26 (m, 3 H), 6.98 (s, 1 H), 5.86 (s, 2 H), 4.72 (d, J = 14.6 Hz, 2 H), 1.79 (d, J = 30.1 Hz, 2 H), 1.46 (d, J = 37.6 Hz, 2 H), 0.93 (d, J = 14.7 Hz, 3 H); ^{13}C-NMR (126 MHz, DMSO-d_6) δ 160.86, 148.10, 145.02, 139.93, 138.16, 137.95, 135.25, 129.06, 129.01, 128.46, 128.24, 127.92, 126.92, 126.64, 125.09, 124.34, 123.13, 123.04, 123.00, 117.77, 113.61, 107.94, 88.93, 56.52, 45.91, 29.40, 19.41, 13.78; HR ESP MS: *m/z*: Found 457.15078 [M+] $C_{28}H_{26}ClN_2S^+$; Requires [M+] 457.1500;

2-((1-benzyl-7-chloroquinolin-4(1 H)-ylidene)methyl)-3-(3-(pyridin-1-ium-1-yl)propyl) benzo[*d*]thiazol-3-ium iodide (**Cl-TO-5**) – (Figs. S13 − 15 / Supporting Information), red solid, yield = 44 %; ^{1}H-NMR (500 MHz, DMSO-d_6) δ 9.14 – 9.10 (m, 2 H), 8.80 (dd, J = 10.9, 8.2 Hz, 2 H), 8.60 (tt, J = 7.7, 1.4 Hz, 1 H), 8.19 – 8.11 (m, 3 H), 8.08 (d, J = 2.0 Hz, 1 H), 7.92 (d, J = 8.4 Hz, 1 H), 7.73 (dd, J = 9.0, 2.0 Hz, 1 H), 7.68 (ddd, J = 8.4, 7.3, 1.3 Hz, 1 H), 7.50 (dd, J = 10.4, 7.5 Hz, 2 H), 7.41 (t, J = 7.3 Hz, 2 H), 7.38 – 7.27 (m, 3 H), 6.93 (s, 1 H), 5.90 (s, 2 H), 4.98 – 4.81 (m, 4 H), 2.60 – 2.51 (m, 2 H); ^{13}C-NMR (126 MHz, DMSO-d_6) δ 160.88, 148.46, 145.70, 145.31, 144.81, 139.78, 138.14, 138.10, 135.24, 135.21, 129.10, 128.45, 128.33, 128.12, 126.95, 126.69, 125.17, 124.36, 123.20, 123.08, 117.83, 113.42, 108.28, 88.90, 57.94, 56.66, 43.12, 28.81; HR ESP MS: *m/z*: Found 648.07448 [M+] $C_{32}H_{28}ClIN_3S^+$; Requires [M+] 648.0732;

2-((7-chloro-1-(3-(4-(dimethylamino)pyridin-1-ium-1-yl)propyl) quinolin-4(1 H)-ylidene) methyl)-3-(3-(pyridin-1-ium-1-yl)propyl) benzo[*d*]thiazol-3-ium iodide (**Cl-TO-6**) – (Figs. S16 − 18 / Supporting Information), red solid, yield = 37 %; ^{1}H-NMR (500 MHz, DMSO-d_6) δ 9.13 (d, J = 6.1 Hz, 2 H), 8.82 (d, J = 9.1 Hz, 1 H), 8.61 (dd, J = 12.0, 7.6 Hz, 2 H), 8.31 (d, J = 7.2 Hz, 2 H), 8.23 (d, J = 1.9 Hz, 1 H), 8.16 (t, J = 7.0 Hz, 1 H), 8.12 (d, J = 7.9 Hz, 1 H), 7.90 (d, J = 8.4 Hz, 1 H), 7.79 (d, J = 8.7 Hz, 1 H), 7.67 (t, J = 7.8 Hz, 1 H), 7.49 (t, J = 7.6 Hz, 1 H), 7.40 (d, J = 7.2 Hz, 1 H), 7.05 (d, J = 7.2 Hz, 2 H), 6.90 (s, 1 H), 4.94 – 4.88 (m, 2 H), 4.84 (t, J = 7.6 Hz, 2 H), 4.65 (t, J = 7.5 Hz, 2 H), 4.37 (t, J = 7.4 Hz, 2 H), 3.18 (s, 6 H), 2.38 (dt, J = 11.7, 5.6 Hz, 4 H); ^{13}C-NMR (126 MHz, DMSO-d_6) δ 160.49, 155.85, 148.46, 145.69, 144.78, 144.69, 141.90, 139.76, 138.48, 138.02, 128.38, 128.11, 126.98, 125.03, 124.17, 123.14, 122.95, 117.25, 113.30, 108.37, 107.78, 88.40, 57.89, 54.01, 51.18, 43.01, 29.75, 28.76; HR ESP MS: *m/z*: Found 848.05542 [M+] $C_{35}H_{37C}lI_2N_5S^+$; Requires [M+] 848.0542;

2.4. Photophysical study of Cl-TO cyanines in organic solvent

The UV–vis spectra were recorded at 25 °C using 10-mm path-length quartz cells on a JASCO V-570 UV–vis-NIR double beam spectrophotometer, equipped with a thermostatic cell holder (Huber MPC-K6 thermostat with precision 1 °C). Steady state fluorescence measurements were performed at room temperature using 10-mm path-length quartz cells on a JASCO FP6600 fluorimeter. Analysis of scientific data and spectral processing were conducted using OriginPro 2019 graphing and analysis software, v. 9.6.0172 (OriginLab Corporation). The photochemical stability was studied in acetonitrile solutions by irradiation at 254 nm in equal intervals of 5 min. The measured absorbance was expressed in % relative to the original intensity.

2.5. UV–vis and spectrofluorimetric interactions with calfthymus-DNA

Calf Thymus-deoxyribonucleic acid – Type I fibres (*Calf Thymus*-DNA) was obtained from Sigma-Aldrich. Tris hydrochloride (Molecular Biology Grade, Ultrapure, Thermo Scientific) and Ethylenediaminetetraacetic acid (Cell Culture Reagent) were purchased from Alfa Aesar. For the nucleic acid interactions, *Calf Thymus*-DNA solution was prepared by dissolution in Tris-EDTA buffer to a final concentration of 1.8658×10^{-2} M, omitting sonication. The aqueous solutions were buffered to pH 7.4 (10 mM Tris − HCl, 0.5 mM EDTA). The DNA concentration per nucleotide can be determined by absorption spectroscopy using the molar absorption coefficient at 258 nm ($\varepsilon = 6.6 \times 10^3$ mol^{-1} dm^3 cm^{-1}) [34]. Dye stock solutions (1 mM) were freshly prepared in DMSO and further diluted with buffer to the appropriate working concentrations. The spectrophotometric and the spectrofluorimetric titrations were performed by adding small aliquots of the deoxyribonucleic acid solution into the solution of the studied monomethine cyanine dyes. All samples were equilibrated at 25 °C for 2 min prior to scanning. The fluorescence emission spectra were recorded at excitation to the longest wavelength absorption maxima (λ_{abs} = 508 − 514 nm). The data from the spectrofluorimetric titrations were processed by the Scatchard equation in order to evaluate the binding constants (*Ks*) of the cyanine dyes to *Calf Thymus* DNA [35,36]. Fitting of the data revealed good correlation, with regression coefficients $R^2 > 0.998$.

2.6. Agarose gel electrophoresis

For the DNA samples, high molecular weight genomic DNA isolated from *Pseudomonas aeruginosa*, plasmid DNA (pUC18) isolated from *Escherichia coli* and DNA size standards Hyperladder I (Bioline), were loaded onto 1 % (w/v) agarose gel and then electrophoresed at 120 V for 45 min in TBE (Tris-Boric acid) buffer. The gel was stained with either **Cl-TO-4** or **Cl-TO-6** dyes (2 μM solution in TBE buffer) and the

gels were visualized using ChemiDoc imager system (Bio-Rad, USA) applying SYBR green filter.

2.7. Cytotoxicity assay

The cytotoxicity (anti-proliferative activity) of the compounds was measured using the methods described previously [37]. MRC5 cells (human lung fibroblast), HCT116 (human colon carcinoma), A549 (human lung carcinoma), MDA-MB-231 (human breast cancer) were all obtained from ATCC and plated in a 96-well flat-bottom plate at a concentration of 1×10^4 cells per well, grown in humidified atmosphere of 95 % air and 5 % CO_2 at 37 °C, and maintained as monolayer cultures in RPMI-1640 medium. After 24 h of incubation, the media containing increasing concentrations of each tested compound (0.1–100 μM) were added to the cells. Control cultures received the vehicle solvent DMSO and blank wells contained 200 μL of growth medium. After 48 h of treatment, cells proliferation was determined using 3-(4,5-dimethylthiazol-2-yl)-2,5-diphenyltetrazolium bromide (MTT) reduction assay. Cell proliferation was determined from the absorbance at 540 nm on Tecan Infinite 200 Pro multiplate reader (Tecan Group, Männedorf, Switzerland). The MTT assay was performed twice in quadruplicate and the results were presented as percentage of the control (untreated cells) that was arbitrarily set to 100 %. The cell viability rate (%) was calculated: (OD of the treated group/OD control group) × 100.

2.8. Fluorescence microscopy

MRC5 cell staining. Upon being plated on microscopic slides (1.5×10^5 cells/slide), human cells were fixed in 4 % paraformaldehyde in PBS (Phosphate-buffered saline) for 20 min at room temperature (RT), washed 3 times with PBS and incubated in 0.25, 0.5 and 5 μM cyanine dyes solutions, for 30 min at room temperature in the dark. Cells were rinsed with PBS, covered with a glass coverslip and analysed. Nuclei were stained with 0.1 mg/mL diamino phenylindole (DAPI; Sigma-Aldrich). The entry and intracellular distribution of tested cyanine dyes were analysed under the fluorescence microscope (Olympus BX51, Applied Imaging Corp., San Jose, USA), under 100 × magnification.

2.9. Flow cytometry analysis of the cell cycle

Fixed and RNAse A treated MRC5 cell line was stained with **Cl-TO-4** and **Cl-TO-6** (1μM solution in PBS) or with propidium iodide (PI; Sigma-Aldrich) (10 μg/mL). The cell cycle phases were analysed by Partec CyFlow Space flow cytometer (Sysmex Partec, Görlitz, Germany) using FL-1 detector (FITC, 525 nm Band Pass Filter) and FL-2 detector (PE and PI, 575 nm Band Pass Filter). The stained cells could be detected in S, G1 and G2 phases.

2.10. Microbial cells staining

Overnight *Candida albicans* (ATCC 10,231) or *Saccharomyces cerevisiae* (baker's yeast from local health food store) cultures were diluted to OD600 = 0.6 and incubated for 3 h at 30 °C. After completion of the incubation period, cells were diluted to 1×10^7 cells/mL, washed twice with PBS, fixed with paraformaldehyde solution (4 %, v/v) and stained with 20 μM of **Cl-TO-4** or **Cl-TO-6** in PBS at RT for 30 min in the dark. Cells were visualized using a fluorescence microscope (Olympus BX51, Applied Imaging Corp., San Jose, USA), under 100 × magnification. *Pseudomonas aeruginosa* (ATCC 10,145) and *Staphylococcus aureus* (ATCC 43,300) strains were grown at 180 rpm and 37 °C in Luria-Bertani broth. Overnight cultures were diluted to OD600 = 0.1 and incubated for 2 h at 37 °C. Microbial cells were harvested by centrifugation, washed twice with PBS, fixed with paraformaldehyde solution (4 %, v/v) and stained with 20 μM of **Cl-TO-4** or **Cl-TO-6** in PBS at room temperature for 30 min in the dark. Cells were visualized using a fluorescence microscope (Olympus BX51, Applied Imaging Corp., San Jose, USA), under 100× magnification. For *Candida* biofilm staining *C. albicans* ATCC 10,231 cells were harvested from overnight grown cultures (Sabouraud broth, 180 rpm, 30 °C) by centrifugation (5000 × g, 5 min, 4 °C), washed twice with sterile phosphate-buffered saline (PBS; Sigma-Aldrich, Munich, Germany), and resuspended in RPMI 1640 medium (Sigma-Aldrich) containing 2 % glucose (w/v) at a concentration of 2×10^6 cells/mL. *C. albicans* suspension was incubated for 48 h at 37 °C without shaking, on a surface of glass cover slips (pretreated with serum for 2 h) in leaning position to allow biofilm at air-liquid interfaces to form. The biofilm was stained with 10 μM of **Cl-TO-4** in PBS at room temperature for 30 min in the dark. Biofilm growth was observed by **Cl-TO-4** staining of adherent cells, under a fluorescence microscope (Olympus BX51, Applied Imaging Corp., San Jose, CA, United States) under 40 × magnification.

3. Results and discussion

3.1. Synthesis of intermediate products and target Cl-TO cyanine dyes

The preparation of intermediates **3a**-**3c** is based on reported procedures for the *N*-quaternization of hetaryl compounds, using an excess of the alkylating agent **2** (methyl iodide - **2a**, butyl iodide - **2b** or 1-(3-iodopropyl)pyridin-1-ium iodide - **2c**) and heating to reflux for 2 h in 2-methoxyethanol serving as the reaction media. All operations were carried out under argon atmosphere in order to hamper possible oxidation or formation of side products. The 2-methylbenzothiazolium salts **3a**-**3c** were obtained in moderate yields varying between 61–72 %. These compounds were found highly hygroscopic, therefore structural identification was achieved on the final dyes. Similarly, derivatives **6a**-**6d** were isolated in good to excellent yields (71–88 %) *via* direct melting for 20 min at 120 °C of the bulk 4,7-dichloroquinoline **4** and a slight excess of the corresponding alkylating reagent **5** (methyl iodide - **5a**, ethyl iodide - **5b**, benzyl bromide - **5c** or 4-(dimethylamino)-1-(3-iodopropyl)pyridin-1-ium iodide - **5d**) under solvent-free reaction conditions. Due to instability of the quinolinium salts, they were prepared and used immediately in the synthesis of the cyanine dyes.

The design of current molecular probes for nucleic acid detection relies on a well-established core of monomethine cyanines. The series of six dyes under investigation represent unsymmetrical mono-, di- and tricationic molecular structures prepared by a condensation reaction between *N*-quaternary benzothiazolium chromophores and chlorine-containing quinolinium salts. The target Cl-TO dyes were obtained suggesting a modified environmentally benign concept as opposed to the classical Brooker's method for cyanine dye synthesis, which features numerous drawbacks (*e.g.* evolution of toxic methane thiol, relatively poor yields, and complex crude product mixtures among others) [38,39]. Previously we reported 3 different reaction procedures for the preparation of TO derivatives using polar protic solvents and sonication (Procedure "A" - methanol, Procedure "B" - water, and Procedure "C" - ethanol) [27]. Among those, both approaches "A" and "B" promoted significant amount of blue coloured by-product. Although ethanol in procedure "C" appears to reduce the quinoline self-condensation, it does not completely hamper the formation. As opposed to previous protocol, our revised synthetic method makes use of a mixture of ethanol (EtOH) : dichloromethane (DCM) at a 3:2 v/v ratio, which was found to improve the reaction yield and afford higher purity of the target monomethines. The formation of bis-quinoline by-product was vanished by current protocol. The reaction proceeds at room temperature employing the sterically hindered *N,N*-diisopropylethylamine (DIPEA -Hünigs base). Recrystallization from absolute ethanol afforded the analytical grade samples of the title dyes. Structural elucidation was held by ^{1}H-NMR, ^{13}C-NMR spectroscopy, and high-resolution mass spectrometry (ESI +).

The design of the Cl-TO series was inspired by previous report on halogenated cyanines, which revealed promising photophysical characteristics. Our efforts were focused to continue the design of the

Table 1
Optical characteristics of the monomethine cyanine dyes in organic media.

Compound	λ_{abs} [a] (nm)	ε ($Lmol^{-1}\ cm^{-1}$)	λ_{fl} [b] (nm)	K_{obs} * (min^{-1})(× 10^{-2})	$t_{1/2}$ * (min)
Thiazole Orange	502	68.500	538	17.20	4.9
Cl-TO-1	509	79.500	548	14.00	8.1
Cl-TO-2	510	82.000	548	9.56	12.6
Cl-TO-3	511	81.400	550	8.75	12.4
Cl-TO-4	514	81.900	553	6.70	13.9
Cl-TO-5	512	80.700	551	3.84	21.6
Cl-TO-6	513	82.000	552	2.95	23.3

[a] UV–vis absorption maximum.
[b] excitation wavelength = λ_{abs}.
* evaluated in acetonitrile.

chlorinated analogues and examine their photophysical properties and staining ability. Initially, minor variations were introduced on the dyes **Cl-TO-1** [27], **Cl-TO-2**, **Cl-TO-3**, and **Cl-TO-4** in order to perform a systematic study on the interactions with DNA. In the case of **Cl-TO-5** and **Cl-TO-6**, incorporation of multiple positive charges aimed to improve water solubility and increase the binding constants between the dye molecules and the double-stranded helix [40–43].

3.2. Evaluation of optical properties of the Cl-TO series in organic media

The photophysical characteristics of the title cyanines were evaluated in methanol using UV–vis and steady state spectrofluorimetric techniques. The well-defined longest wavelength absorption maxima (λ_{abs}) of the Cl-TO dyes were registered between 509 − 514 nm, the fluorescence emission maxima (λ_{fl}) were allocated around 548 − 553 nm, while the corresponding molar extinction coefficients (ε) were evaluated from 79.500 to 82.000 mol dm^{-3} cm^{-1}. The optical characteristics are summarized in Table 1.

In comparison to the parental Thiazole Orange, the introduction of a chlorine atom to the C-7 position to the quinolinium chromophore resulted in a small bathochromic shift ($\Delta\lambda$ = 7 nm for **Cl-TO-1**), which fits to the Woodward-Fieser empirical rules [44,45]. Further variations of the *N*-alkyl substituents of **Cl-TO-2**, **Cl-TO-3** and **Cl-TO-6** barely affected the position of the maxima. The presence of a benzyl group was found to apply additional minor red shift in the cases of the cyanines **Cl-TO-4** and **Cl-TO-5**. Similarly, the fluorescence emission maxima were shifted towards the lower energies by approximately 10 − 15 nm.

The ability of a chromophore to resist against photooxidative destruction is a highly desired property. Singlet oxygen produced *in situ* by irradiation of the dyes can be added to the conjugated system, leading to a disruption of the conjugation, causing photobleaching. Photobleaching is related to the kinetic stability of the dye molecules in solution under atmospheric oxygen and continuous exposure to UV-irradiation. According to several reports, intersystem crossing yields are rather poor for cyanine dyes. However, this class of organic molecules is known to rapidly react with singlet oxygen [46]. Therefore, such kind of processes are very important and should not be underestimated when designing new chromophores.

For the purpose of our current study, we used the commercial product Thiazole Orange (tosylate) without attempting further modifications. We intended to do a direct comparison of the newly synthesized dyes to the conventional nucleic acid stain. Methanol and acetonitrile are the most frequently employed solvents for “forced degradation studies” [47,48]. Acetonitrile was used to perform the photostability tests in order to avoid hydrogen abstraction, or any other photo catalytic reactions related to the nature of the polar protic alcohol. Fig. 2A illustrates the comparative resistance to photooxidative destruction of the dyes by continuous irradiation (over 5-minute intervals) with a strong UV-light. The position of the longest wavelength absorption maxima remained unchanged until reaching complete

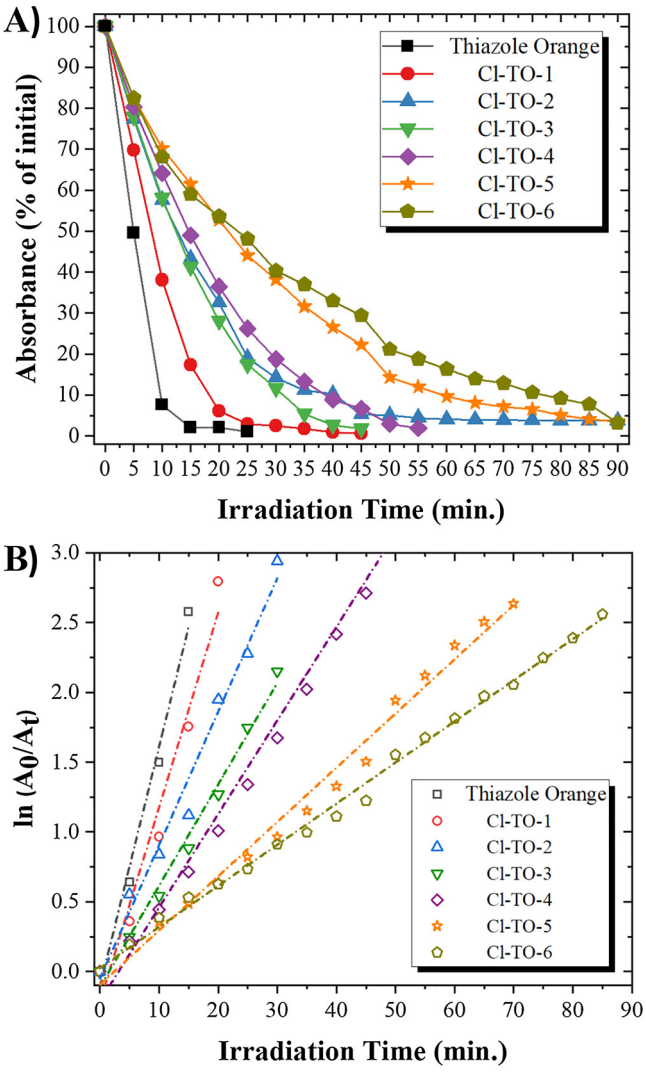

Fig. 2. Photobleaching decay curve of the studied cyanine dyes (panel A), and pseudo-first order linear representation of ln A_0/A_t against the irradiation time (panel B).

discoloration of the solutions. The photodegradation of the dyes obeys a pseudo-first order kinetics. The corresponding correlation coefficients of the tendency lines were evaluated between 0.97 − 0.99. In order to obtain further information on the parameters of the photodegradation process, the following kinetic relationship was used :

$$r = -\frac{dC}{dt} = K_{obs}C \quad (1)$$

where, C represents the concentration of the cyanine dye and K_{obs} is the observed first-order rate constant [49,50]. As shown in Eq. 2, the concentration-time dependence was formed from the integration of the previous expression.

$$\ln\left(\frac{C_0}{C_t}\right) = K_{obs}t_{1/2} \quad (2)$$

According to the Lambert-Beer law, the absorbance is proportional to the concentration. Substituting the concentration C variable with that of the absorbance A at maximal wavelength, and bearing in mind the unchanged spectral shape upon irradiation, Eq. 3 can be derived [51]:

$$\ln\left(\frac{A_0}{A_t}\right) = K_{obs}t_{1/2} \quad (3)$$

The plot of ln(A_0/A_t) against the irradiation time (Fig. 2B) shows the

angular coefficient, which equals the rate constant K_{obs} of the photodegradation process. The half-life ($t_{1/2}$) of the title monomethines was found up to 5 times greater than the commercially available Thiazole Orange ($t_{1/2}$ = 23.3 min for **Cl-TO-6**, $t_{1/2}$ = 4.9 min in the case of TO). Early works of Armitage and co-workers also suggest, that halogenated Thiazole Orange derived dyes (fluorine containing analogues) exhibit increased oxidation potential and are less reactive towards singlet oxygen [52]. With respect to the counterion, several articles report enhanced photostabilization of the I^- over that of the TsO^- (tosylate) counter ion [53]. Perhaps attraction between the π-bonds of the benzene ring in the tosylate anion and the π -bonds of the cyanine dye are responsible for energy transfer between the ion pair causing photobleaching. On the other hand, small hard anions are prone to have a quenching effect on the singlet oxygen formed during the photodynamic process [54–56]. Previously we conducted a direct comparison between a synthesized TO cyanine and its chlorinated analogue (both dyes carrying iodide counter ion). The results proved comparable photostability between the two dyes [29]. Superior resistance to the photodegradation was observed on the addition of extra charges to the molecular structure. The 4-fold enhanced photostability for **Cl-TO-5** and 5-fold in the case of **Cl-TO-6** ($t_{1/2}$ = 21.6 min and $t_{1/2}$ = 23.3 min respectively), might be attributed to the increased number of inorganic counterions consuming the formed singlet oxygen. The two multicationic cyanines reach complete discoloration after about 90 min of irradiation with UV-light.

3.3. UV–vis and fluorescence titrations of the free Cl-TO monomethine cyanine dyes and association to Calf Thymus-DNA in buffer solutions

Concentration dependent studies of the free dyes were held in aqueous buffer media to monitor the spectral shape, allocate the absorption maxima (λ_{abs}), and evaluate the molar absorptivities (ε). All experiments were performed at a micromolar range. The UV–vis spectra of the buffered solutions revealed a good linear correlation, with regression coefficients $R^2 > 0.98$. The Beer-Lambert law was examined and found to be valid over the concentration range of 1 − 12 μM, where no systematic deviation could be observed (Fig. S19). Therefore, the possibility of self-association between the dye molecules was neglected. The Cl-TO compounds were characterized by a typical broad single-peak absorption band ranging approximately between 400 − 580 nm. The longest wavelength absorption maxima of the title dyes were registered between 508 nm and 514 nm, while the molar absorptivities were evaluated to be 67.900-74.100 L mol^{-1} cm^{-1}. The position of the λ_{abs} were almost identical to those observed in methanol. The evaluated optical characteristics of the monomethine cyanine dyes are summarized in Table 2.

In order to evaluate the affinity of the synthesized molecules towards DNA, we conducted spectrophotometric and fluorimetric titrations. The interactions of the Cl-TO monomethine cyanines with nucleic acids were studied in TE aqueous buffer solutions (10 mM Tris − HCl / 0.5 mM EDTA, pH 7.4). The titrations revealed homogeneous changes to the absorbance bands. The increase of the *Calf Thymus*-DNA concentration resulted in a continuous decrease of the absorption intensity (Fig. 3A and Fig. S20). The attenuation of the absorption maxima (up to 39 % hypochromism) was accompanied by a moderate bathochromic shift ($\Delta\lambda$ = +7 nm) until saturation of the binding was reached. This

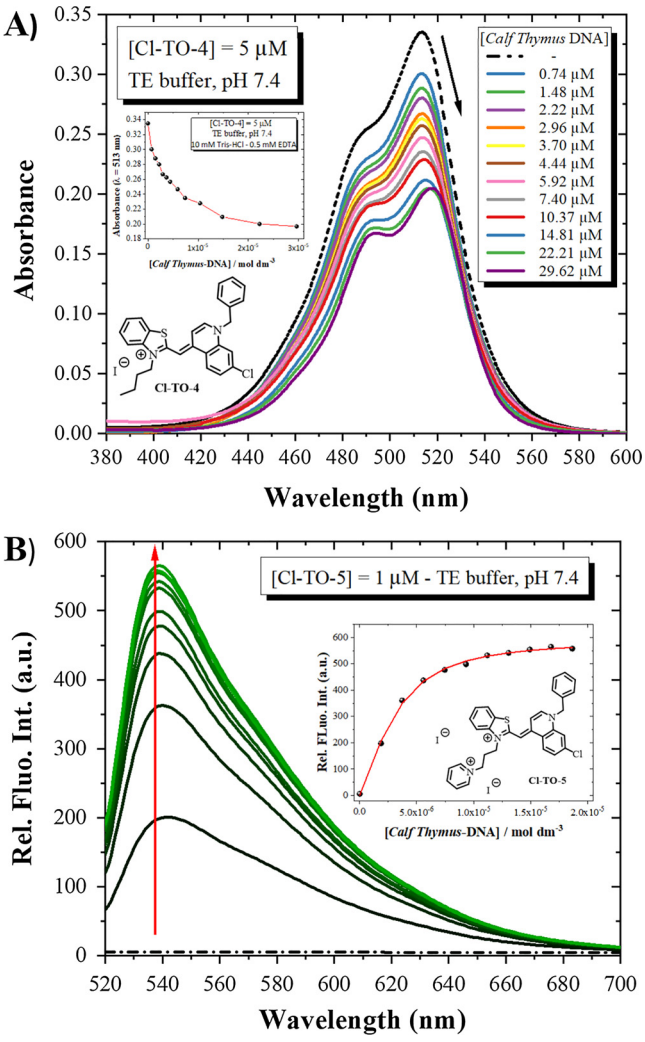

Fig. 3. Spectrophotometric titration between Calf Thymus-DNA and **Cl-TO-4** (panel A), and fluorometric titration of the **Cl-TO-5** dye (panel B). Shown in inset to the right is the binding isotherm processed by the Scatchard equation at 538 nm.

Table 2
Optical characteristics of the cyanine dyes in the presence of *Calf Thymus-DNA* in TE buffer solutions (10 mM Tris − HCl / 0.5 mM EDTA), pH 7.4, T = 25 °C.

Compound	λ_{abs} [a] (nm)	λ_{fl} [b] (nm)	ε ($Lmol^{-1}$ cm^{-1})	ΔI calc. [c]	Ks ($\times 10^6$)	log Ks	n ± error
Thiazole Orange	502	526	63.000	252	1.55	6.19	0.25 ± 0.04
Cl-TO-1	508	534	74.100	211	2.22	6.35	0.24 ± 0.02
Cl-TO-2	509	536	67.900	270	2.16	6.34	0.17 ± 0.02
Cl-TO-3	510	536	68.300	150	1.26	6.10	0.25 ± 0.06
Cl-TO-4	513	540	70.400	261	6.32	6.80	0.20 ± 0.04
Cl-TO-5	511	538	69.600	834	4.56	6.66	0.18 ± 0.02
Cl-TO-6	514	539	72.900	499	4.76	6.68	0.15 ± 0.01

[a] UV–vis absorption maximum of the free dyes.
[b] Fluorescence emission maximum upon excitation at λ_{abs}.
[c] Changes in the fluorescence signal (ΔI calc. = I / I_0, where I is the maximum fluorescence emission intensity of the dye-DNA complex, while I_0 represents the fluorescence emission intensity of the free dye.

observation presumably accounts for strong interaction of the monomethines with the double stranded helix. Similar red shift of 8 nm was previously reported for the intercalating agent Thiazole Orange by Prodhomme *et. al.* [57].

Cyanine dyes have a strong tendency to form H- or J-type of self-associates due to π-stacking. This phenomenon is favored when performing studies in highly viscous solvents or in the presence of hydrophobic host molecules with appropriate cavity size [58–61]. The formation of self-associates is typically followed by the appearance of new absorption bands in the UV–vis spectrum. The spectral shape of the Cl-TO compounds remained unaltered in the presence of DNA which led us to assume, that the title cyanines are bound as monomers. Usually, pronounced decrease in the absorption intensity and bathochromically shifted λ_{max} is an evidence for the "intercalation" of a small molecule between the DNA base pairs [62–66]. On the other hand, the hydrophobic pockets of the beta-helix are relatively wide and deep to accommodate small molecules (DNA width =11.7 Å – major groove, 5.7 Å minor groove / depth =8.5 Å – major groove, 7.5 Å – minor [67]). Groove binding of a single dye molecule is also not an unknown aspect. Monomeric "groove binders" typically resemble crescent shape. Classical examples involve the Hoechst33258, BOXTO, netropsin, distamycin, berenil, and the furamidine derivative DB293, which strongly bind pure AT-rich sequences [68–74]. Since both, the "intercalation" and the latter "groove binding" motifs could potentially exhibit similar spectral behavior, the spectrophotometric data is insufficient to rule out any of them.

In parallel to the UV–vis measurements, we performed spectrofluorimetric studies in order to assess the fluorescent labelling ability of the newly synthesised dyes. The experimental part was carried out in a similar way to the spectrophotometric experiments. An excess of the polynucleotides was applied over that of the monomethine chromophores. Intrinsically non-emittive in aqueous solution, the Cl-TO cyanines acquired strong fluorescence signal after incubation with *Calf Thymus*-DNA. The addition of increasing amounts of DNA, resulted in the continuous increase of the fluorescence emission signal intensity till saturation of binding was reached. The I/I_0 ratios were evaluated between 211–270 for the monocationic analogues **Cl-TO-1**, **Cl-TO-2**, and **Cl-TO-4**. On the other hand, the di- and tricationic **Cl-TO-5** and **Cl-TO-6** cyanines exhibited approximately 2–3 times greater increase of the fluorescence emission response compared to the parental Thiazole Orange. Shown in Fig. 3B is the titration of the **Cl-TO-5** with *Calf Thymus*-DNA, which revealed an 834-fold signal enhancement. The experimental data were processed using the Scatchard equation for the evaluation of the binding sites *n*, and to calculate the stability constants *Ks*. The fitting of the data showed good correlation, with regression coefficients $R^2 > 0.998$. The binding parameters are summarized in Table 2. The spectrofluorimetric titrations gave ratios *n* between 0.15 − 0.25. Following the nearest neighbour exclusion principle, *n* values of 0.25 represent saturation of the available intercalative binding sites of DNA as reported for Thiazole Orange [75–77]. Depending on the dye chemical structure, the binding constants of the Cl-TO analogues to the double-stranded helix vary between 1.26×10^6 - 6.32×10^6. The calculated *Ks* values were found to be higher than several reported DNA fluorescent stains, such as phenanthridine, fluorene and TO derived probes [78–81]. Comparable fluorescence response and binding constants were observed for the monocationic dyes **Cl-TO-1** and **Cl-TO-2**. Apparently, varying the substituent on the benzothiazole only (from *N*-methyl to the longer *N*-butyl) did not affect the binding parameters. However, a minor alternation of the alkyl sidechain on the quinolinium heterocycle (form *N*-methyl to *N*-ethyl in the case of **Cl-TO-3**) was responsible for decreasing both *ΔI* and *Ks*. Intriguingly, the *N*-benzyl substituted monocationic **Cl-TO-4** bound to *Calf Thymus*-DNA, revealed similar fluorescence response to **Cl-TO-1** and **Cl-TO-2**, but the binding constant was significantly larger ($Ks = 6.32 \times 10^6$). The *Ks* values of the multicationic **Cl-TO-5** and **Cl-TO-6** cyanines were found to be greater than the single charged molecules (except **Cl-TO-4**). Approximately 2–3 times higher *Ks* were evaluated for the di- and tricationic compounds compared to the dyes featuring pure alkyl sidechains.

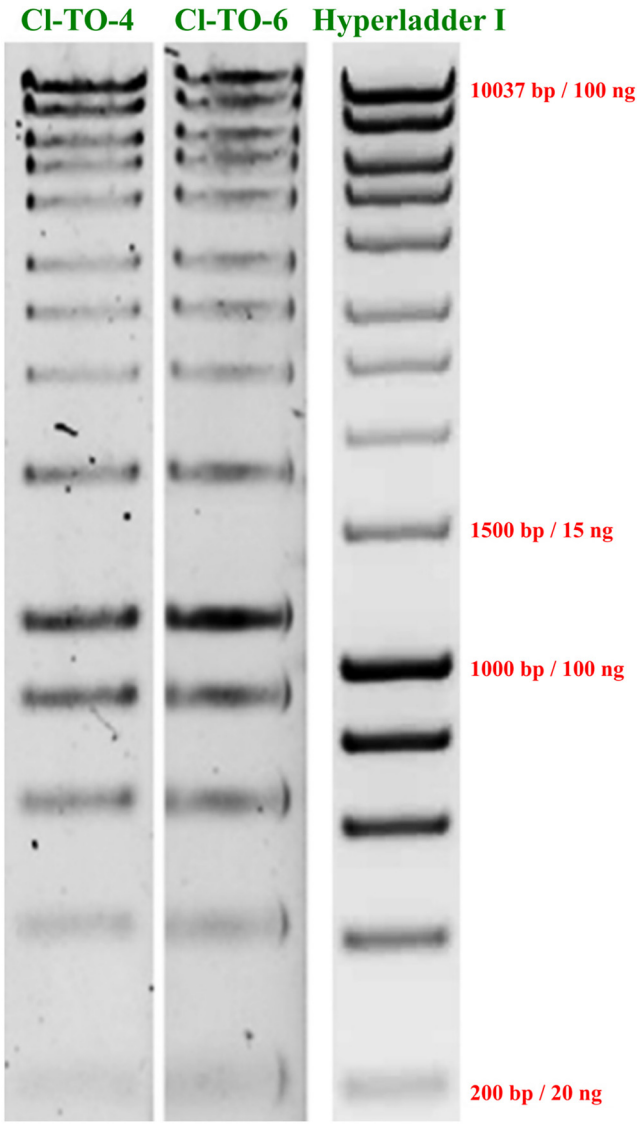

Fig. 4. Agarose gel electrophoresis (1%, w/v) of Hyperladder I standard DNA (Bioline) stained with **Cl-TO-4** and **Cl-TO-6** in comparison to commercial EtBr (Ethidium Bromide) staining (https://www.bioline.com/hyperladder-1kb.html.

Table 3
Cytotoxic effects of the dyes on various cancer cell lines expressed as the IC50 values (μM).

IC50[a], μM	MRC5 normal	HCT116 colon	A549 lung	MDA-MB-231 breast
Thiazole Orange	0.5	0.8	1.5	2
Cl-TO-1	2	2	2	2
Cl-TO-2	2	2	2	2
Cl-TO-3	2.5	2	2	2
Cl-TO-4	1.8	2	2	2
Cl-TO-5	20	20	40	40
Cl-TO-6	50	55	80	80

[a] IC50 – the concentration inhibiting 50 % of cell growth after treatment with the test compounds. Values were determined as quadruplicate of three independent experiments with SD values between.1–3 %.

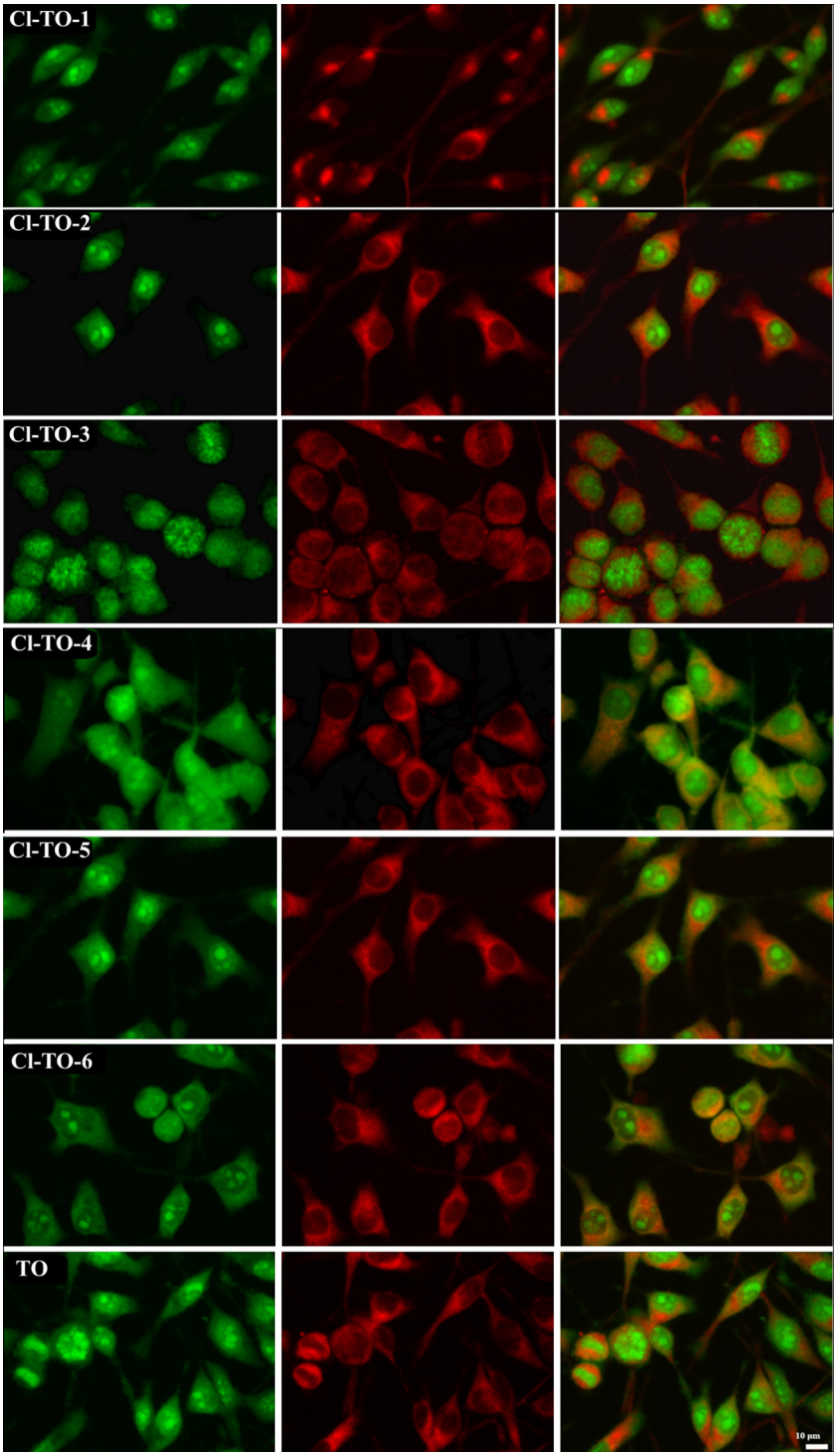

Fig. 5. MRC5 cells stained with the Cl-TO derivatives and Thiazole Orange coupled with CellTracker Red CMTPX (fluorescent dye suited for whole-cell detection). Fixed cells were stained using 1 μM dyes for 30 min and analyzed under fluorescent microscope (green: FITC channel for cyanine dyes and red: Texas Red channel for red tracker dye; 100 × magnification).

3.4. Agarose gel electrophoresis

The monomethines **Cl-TO-4** and **Cl-TO-6** were also used in staining a variety of DNA molecules after their separation by agarose gel electrophoresis (Fig. 4 and Fig. S22).

These two dyes were very competent in post-electrophoretic visualization of both types of double-stranded DNA, plasmid (pUC18) DNA that is a small supercoiled and circular and bacterial genomic DNA of high molecular weight. The staining efficiency and detection limits of both Cl-TO derivatives were comparable to that of widely used Ethidium Bromide (EtBr), as 20 ng of 200 bp as well as 15 ng of 1500 bp long DNA fragments were clearly observable after gel electrophoresis using Cl-TO and EtBr staining.

3.5. Cytotoxicity assay

Nucleic acid targeting compounds usually appear to be highly cytotoxic. Such action mode is often observed in several classes of anti-

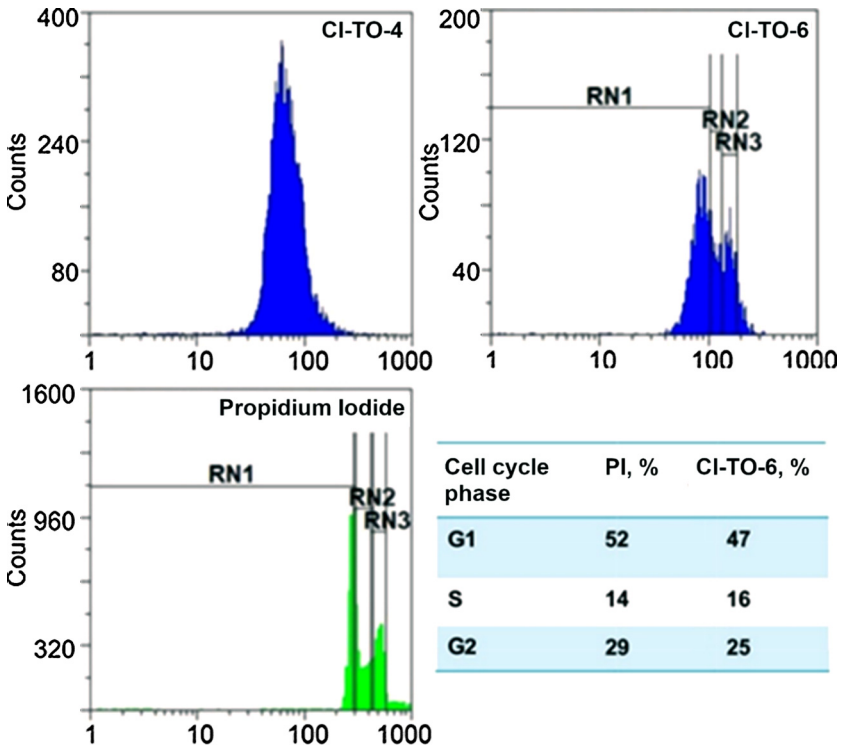

Cell cycle phase	PI, %	Cl-TO-6, %
G1	52	47
S	14	16
G2	29	25

Fig. 6. Flow cytometric analysis of cell cycle distribution in MRC5 cells stained with 1 μM of **Cl-TO-4** or **Cl-TO-6** and propidium iodide (PI; 10 μg/mL) for 30 min. Cell cycle analysis was performed on an equal number of MRC5 cells (10^6). The cells were ethanol fixed, RNase A treated and stained. The stained cells could be detected in G1, S and G2 phases with % of cell population given in table form. FACS analysis was done by Partec CyFlow Space flow cytometer.

cancer agents. In the present study we have evaluated the antiproliferative activity of Thiazole Orange and its six chlorinated derivatives (**Cl-TO-1**, **Cl-TO-2**, **Cl-TO-3**, **Cl-TO-4**, **Cl-TO-5** and **Cl-TO-6**) against normal human lung fibroblasts (MRC5) and a panel of three human cancer cell lines included non-small cell lung carcinoma (A549), colon carcinoma (HCT116) and breast cancer (MDA-MB231). The IC50 concentration values of the monomethine cyanine dyes obtained after 48 h cell exposure are presented in Table 3.

The halogenated cyanines exhibited cytotoxic activity in the concentration range from 1.8–80 μM on all cell lines. All newly synthesised compounds were found to be less cytotoxic against healthy human fibroblasts (MRC5) in comparison to the TO from 3.6 to 100 times. The lowest cytotoxicity was exhibited by **Cl-TO-6** followed by **Cl-TO-5** across all tested cell lines. The monocationic derivatives were comparably cytotoxic to the TO with IC50 values in the range from 1.8 to 2.5 μM. In comparison, IC50 values of 21 μM for A549 and 18 μM for MRC5 cells are reported in the literature for the conventional heptamethine cyanine IR-780 [82].

3.6. Fluorescence microscopy

Moderate to low cytotoxicity of these dyes could be their advantage in applications as cellular fluorescent probes. All Cl-TO derivatives were suitable for cell staining (1 μM solution, 30 min) and visualization under fluorescent microscope (Fig. 5). Concentration of 1 μM was chosen according to their cytotoxic effects on treated human cell lines (Table 3), however lower concentrations such as 0.25 and 0.5 μM provided stable staining intensity (Fig. S23). From counterstaining with CellTracker Red probe, which distributes throughout cell cytoplasm, the preferential specificity of Cl-TO dyes to nuclei was demonstrated although they are also present in the cytoplasm. The observed distribution could be due to the differential preference between DNA and RNA molecules. **Cl-TO-2** and **Cl-TO-3** are highly selective towards the nucleus with **Cl-TO-3** stained the chromosomes efficiently in MRC5 cell lines. The careful study of these images revealed that some areas of nuclei were more compactly stained with **Cl-TO-1**, **Cl-TO-2**, **Cl-TO-5** and **Cl-TO-6**. These may be the regions of condensed chromatin, heterochromatin, part of the chromosomes, which is a firmly packed and considered genetically inactive [83].

3.7. Flow cytometry analysis of the cell cycle

Cyanines **Cl-TO-4** and **Cl-TO-6** were used in flow cytometry analysis of cell cycle using MRC5 cell line at 1 μM or with PI (10 μg/mL) (Fig. 6). The monomethine cyanine **Cl-TO-6** manifested great potential to be used for evaluation of the number of cells in G1, S and G2 phases with comparable efficiency with widely used PI (Propidium Iodide) [84]. However, **Cl-TO-4** was not suitable for this purpose, indicating differential behaviour towards living non-permeabilized cells.

3.8. Microbial cells staining

Cl-TO-4 appeared to localize predominantly with cell material, while **Cl-TO-6** was dispersed (Fig. S24). The two dyes were examined for their ability to stain wide selection of microbial cells, as well (Fig. 7). The monomethine derivative **Cl-TO-4** was able to stain all microbial cells (*C. albicans*, *S. cerevisiae*, *P. aeruginosa* and *S. aureus*) more efficiently than **Cl-TO-6**, although microbial cell selection included Gram-positive, Gram-negative, fungal and eukaryotic representatives with distinct differences in cell membrane and envelope. Efficient fluorescent staining of microbial cells is of great importance for their counting and sorting using flow cytometry approach [85–88]. **Cl-TO-4** dye could also be successfully used to stain *C. albicans* biofilms preformed on glass cover slips (Fig. S25). Notably, TO is also suitable for similar type of microbial staining (Fig. 7), however given its higher cytotoxicity, Cl-TO dyes are deemed as more suitable for this application.

4. Conclusions

In summary, this paper reports the synthesis of monomethine cyanine series suggesting an advanced synthetic protocol. Elucidation of all chemical structures was achieved employing NMR spectroscopy and high-resolution mass spectrometry (ESI+). The title compounds

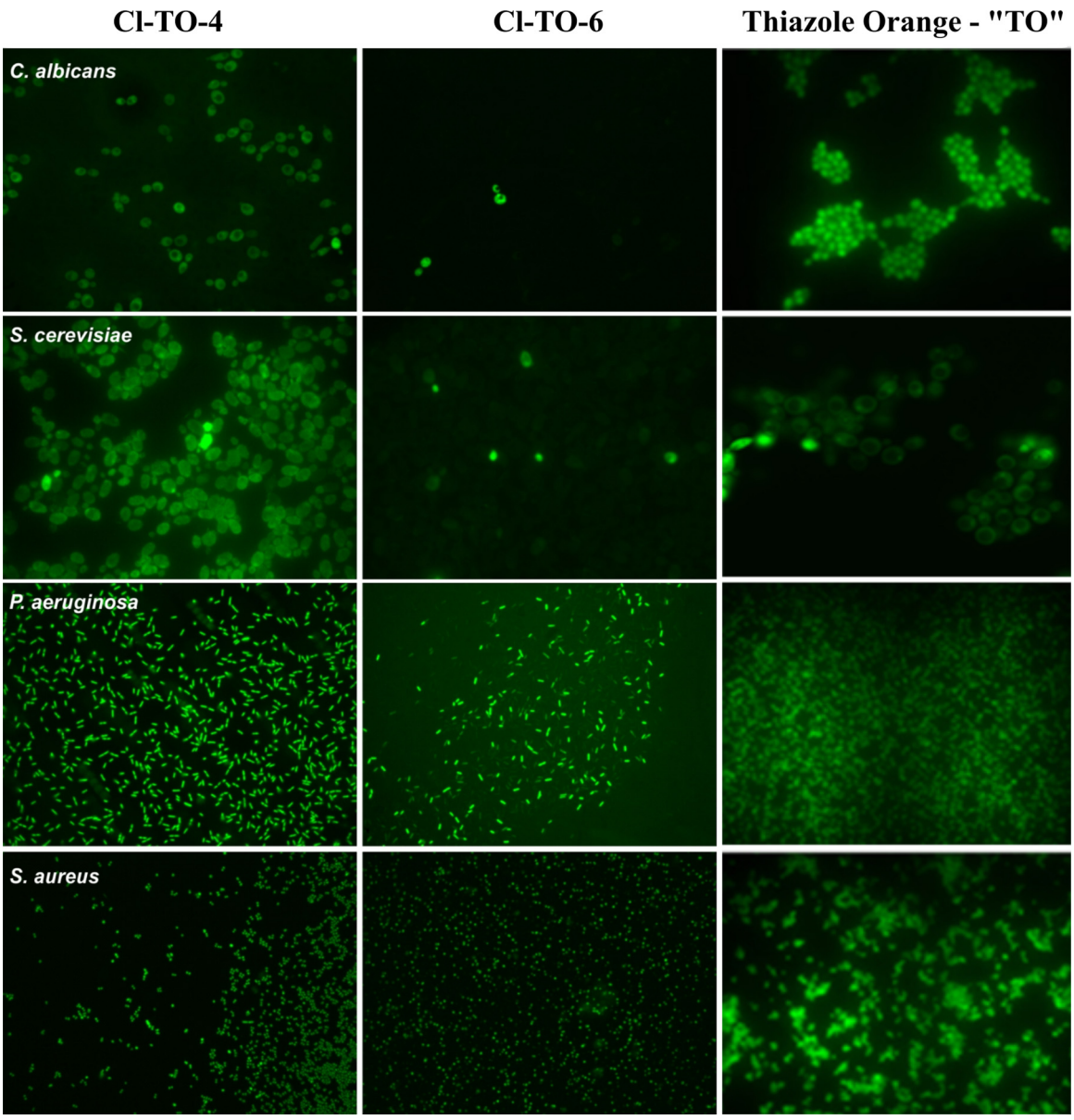

Fig. 7. Microbial cells stained with **Cl-TO-4**, **Cl-TO-6** and **TO** visualized under fluorescent microscope (FITC channel; 100 × magnification). Candida albicans, Saccharomyces cerevisiae, *Pseudomonas aeruginosa* and *Staphylococcus aureus* cells were fixed and stained with 20 μM dyes.

manifested improved resistance against photobleaching, and higher molar extinction coefficients compared to the commercially available Thiazole Orange. Up to 5-fold increased photostability was observed for the Cl-TO series as opposed to the conventional fluorescent probe. The title compounds were screened as fluorescent markers for nucleic acid detection. The UV–vis and spectrofluorimetric studies provided clear evidence for strong interactions with biomacromolecules at micromolar concentrations. Significant fluorescence enhancement was observed among all chlorinated monomethines - up to 834-fold increase of the fluorescence emission signal. The observed differences in the ΔI and the Ks magnitudes were found to be dependent on the dye chemical structure. The multicationic monomethines exhibited greater fluorescence enhancement and higher stability constants compared to the single charged TO analogues. The results from the spectroscopic titrations allowed as to recommend the current non-cytotoxic compounds as good potential candidates for DNA staining. Agarose gel electrophoresis showed that the staining efficiency and detection limits of the tested Cl-TO derivatives is comparable to the widely used Ethidium Bromide (EtBr). The results from the flow cytometry revealed great potential for the Cl-TO-6 dye used in G1, S and G2 phases of the cell cycle analysis. The applicability of the synthesized fluorogenic dyes for staining both eukaryotic and microbial cells was also demonstrated. The experimental findings further advance our knowledge on future design and development of fluorogenic platforms for biological applications.

Authorship statement

All persons who meet authorship criteria are listed as authors, and all authors certify that they have

participated sufficiently in the work to take public responsibility for the content, including participation in

the concept, design, analysis, writing, or revision of the manuscript. Furthermore, each author certifies that

this material or similar material has not been and will not be submitted to or published in any other

publication before its appearance in the *Journal of Photochemistry and Photobiology A: Chemistry*.

Authorship contributions

Please indicate the specific contributions made by each author (list the authors' initials followed by their
surnames, *e.g.*, Y.L. Cheung). The name of each author must appear at least once in each of the three
categories below.

Category 1

Conception and design of study: A. Kurutos, J. Nikodinovic-Runic;
acquisition of data: A. Kurutos, T. Ilic-Tomic, F. S. Kamounah, A. A. Vasilev, J. Nikodinovic-Runic;
analysis and/or interpretation of data: A. Kurutos, T. Ilic-Tomic, J. Nikodinovic-Runic;

Category 2

Drafting the manuscript: A. Kurutos, J. Nikodinovic-Runic;
revising the manuscript critically for important intellectual content: A. Kurutos, J. Nikodinovic-Runic;

Category 3

Approval of the version of the manuscript to be published (the names of all authors must be listed): A. Kurutos, T. Ilic-Tomic, F. S. Kamounah, A. A. Vasilev, J. Nikodinovic-Runic.

Acknowledgements

The financial support by the Bulgarian National Science Fund (BNSF) under grant – "Novel monomethine cyanine dyes as potential non-covalent biomarkers: synthesis, evaluation, and studies on photophysical properties" contract № DM09/5 from 17.12.2016 is gratefully acknowledged by AK for the preparation of the compounds Cl-TO-1, Cl-TO-2, Cl-TO-3, Cl-TO-4, the photophysical studies and the interactions of all dyes with DNA. This research has also been financially supported by the Ministry of Education, Science and Technological Development of the Republic of Serbia, under Grant No. 173048. AV gratefully acknowledge the Bulgarian National Science Fund (BNSF) project SOFIa (KP-06-H39/11) from 09.12.2019 for the support in preparation of dyes Cl-TO-5 and Cl-TO-6.

Appendix A. Supplementary data

Supplementary material related to this article can be found, in the online version, at doi:https://doi.org/10.1016/j.jphotochem.2020.112598.

References

[1] E.A. Owens, H. Hyun, T.L. Dost, J.H. Lee, G. Park, D.H. Pham, M.H. Park, H.S. Choi, M. Henary, Near-infrared illumination of native tissues for image-guided surgery, J. Med. Chem. 59 (2016) 5311–5323, https://doi.org/10.1021/acs.jmedchem.6b00038.

[2] J. Cha, R.R. Nani, M.P. Luciano, G. Kline, A. Broch, K. Kim, J.-M. Namgoong, R.A. Kulkarni, J.L. Meier, P. Kim, M.J. Schnermann, A chemically stable fluorescent marker of the ureter, Bioorg. Med. Chem. Lett. 28 (2018) 2741–2745, https://doi.org/10.1016/j.bmcl.2018.02.040.

[3] A. Kurutos, I. Orehovec, A. Tomašić Paić, I. Crnolatac, L. Horvat, N. Gadjev, I. Piantanida, T. Deligeorgiev, New series of non-toxic DNA intercalators, mitochondria targeting fluorescent dyes, Dye. Pigment. 148 (2018) 452–459, https://doi.org/10.1016/j.dyepig.2017.09.049.

[4] A. Kumar Das, H. Ihmels, S. Kölsch, Diphenylaminostyryl-substituted quinolizinium derivatives as fluorescent light-up probes for duplex and quadruplex DNA, Photochem. Photobiol. Sci. 18 (2019) 1373–1381, https://doi.org/10.1039/C9PP00096H.

[5] A. Kurutos, I. Orehovec, D. Saftić, L. Horvat, I. Crnolatac, I. Piantanida, T. Deligeorgiev, Cell penetrating, mitochondria targeting multiply charged DABCO-cyanine dyes, Dye. Pigment. 158 (2018) 517–525, https://doi.org/10.1016/j.dyepig.2018.05.035.

[6] H.-J. Chen, C.Y. Chew, E.-H. Chang, Y.-W. Tu, L.-Y. Wei, B.-H. Wu, C.-H. Chen, Y.-T. Yang, S.-C. Huang, J.-K. Chen, I.-C. Chen, K.-T. Tan, S-cis diene conformation: a new bathochromic shift strategy for near-infrared fluorescence switchable dye and the imaging applications, J. Am. Chem. Soc. 140 (2018) 5224–5234, https://doi.org/10.1021/jacs.8b01159.

[7] M.A. Fomin, R.I. Dmitriev, J. Jenkins, D.B. Papkovsky, D. Heindl, B. König, Two-acceptor cyanine-based fluorescent Indicator for NAD(P)H in tumor cell models, ACS Sens. 1 (2016) 702–709, https://doi.org/10.1021/acssensors.5b00315.

[8] E. De los Reyes-Berbel, R. Salto-Gonzalez, M. Ortega-Muñoz, F.J. Reche-Perez, A.B. Jodar-Reyes, F. Hernandez-Mateo, M.D. Giron-Gonzalez, F. Santoyo-Gonzalez, PEI-NIR heptamethine cyanine nanotheranostics for tumor targeted gene delivery, Bioconjugate Chem. 29 (2018) 2561–2575, https://doi.org/10.1021/acs.bioconjchem.8b00262.

[9] G. Knorr, E. Kozma, J.M. Schaart, K. Németh, G. Török, P. Kele, Bioorthogonally applicable fluorogenic cyanine-tetrazines for No-Wash super-resolution imaging, Bioconjugate Chem. 29 (2018) 1312–1318, https://doi.org/10.1021/acs.bioconjchem.8b00061.

[10] V. Vinatier, V. Guieu, Y. Madaule, M. Maturano, C. Payrastre, P. Hoffmann, Superoxide-induced bleaching of streptocyanine dyes: application to assay the enzymatic activity of superoxide dismutases, Anal. Biochem. 405 (2010) 255–259, https://doi.org/10.1016/j.ab.2010.06.006.

[11] N. Melnychuk, A.S. Klymchenko, DNA-functionalized dye-loaded polymeric nanoparticles: ultrabright FRET platform for amplified detection of nucleic acids, J. Am. Chem. Soc. 140 (2018) 10856–10865, https://doi.org/10.1021/jacs.8b05840.

[12] P. Klimkowski, S.D. Ornellas, D. Singleton, A.H. El-Sagheer, T. Brown, Design of thiazole orange oligonucleotide probes for detection of DNA and RNA by fluorescence and duplex melting, Org. Biomol. Chem. 17 (2019) 5943–5950, https://doi.org/10.1039/C9OB00885C.

[13] H.S. Rye, S. Yue, D.E. Wemmer, M.A. Quesada, R.P. Haugland, R.A. Mathies, A.N. Glazer, Stable fluorescent complexes of double-stranded DNA with bis-intercalating asymmetric cyanine dyes: properties and applications, Nucleic Acids Res. 20 (1992) 2803–2812, https://doi.org/10.1093/nar/20.11.2803.

[14] T.-C. Wang, F. Cochet, F.A. Facchini, L. Zaffaroni, C. Serba, S. Pascal, C. Andraud, A. Sala, F. Di Lorenzo, O. Maury, T. Huser, F. Peri, Synthesis of the new cyanine-labeled bacterial lipooligosaccharides for intracellular imaging and in vitro microscopy studies, Bioconjugate Chem. 30 (2019) 1649–1657, https://doi.org/10.1021/acs.bioconjchem.9b00044.

[15] A.B. Braun, I. Wehl, D.K. Kölmel, U. Schepers, S. Bräse, New polyfluorinated cyanine dyes for selective NIR staining of mitochondria, Chem. Eur. J. 25 (2019) 7998–8002, https://doi.org/10.1002/chem.201900412.

[16] W. Meng, Y. Chen, Y. Feng, H. Zhang, Q. Xu, M. Sun, W. Shi, J. Cen, J. Zhao, K. Xiao, An off–on fluorescent probe for the detection of mitochondria-specific protein persulfidation, Org. Biomol. Chem. 16 (2018) 6350–6357, https://doi.org/10.1039/C8OB01608A.

[17] A. Mishra, R.K. Behera, P.K. Behera, B.K. Mishra, G.B. Behera, Cyanines during the 1990s: a review, Chem. Rev. 100 (2000) 1973–2012, https://doi.org/10.1021/cr990402t.

[18] Z. Lou, P. Li, K. Han, Redox-responsive fluorescent probes with different design strategies, Acc. Chem. Res. 48 (2015) 1358–1368, https://doi.org/10.1021/acs.accounts.5b00009.

[19] J.B. Wu, C. Shi, G.C.-Y. Chu, Q. Xu, Y. Zhang, Q. Li, J.S. Yu, H.E. Zhau, L.W.K. Chung, Near-infrared fluorescence heptamethine carbocyanine dyes mediate imaging and targeted drug delivery for human brain tumor, Biomaterials. 67 (2015) 1–10, https://doi.org/10.1016/j.biomaterials.2015.07.028.

[20] G.-Y. Pan, H.-R. Jia, Y.-X. Zhu, R.-H. Wang, F.-G. Wu, Z. Chen, Dual channel activatable cyanine dye for mitochondrial imaging and mitochondria-targeted Cancer theranostics, ACS Biomater. Sci. Eng. 3 (2017) 3596–3606, https://doi.org/10.1021/acsbiomaterials.7b00480.

[21] F. Xue, Y. Wen, P. Wei, Y. Gao, Z. Zhou, S. Xiao, T. Yi, A smart drug: a pH-responsive photothermal ablation agent for Golgi apparatus activated cancer therapy, Chem. Commun. 53 (2017) 6424–6427, https://doi.org/10.1039/C7CC03168H.

[22] S. Luo, E. Zhang, Y. Su, T. Cheng, C. Shi, A review of NIR dyes in cancer targeting and imaging, Biomaterials. 32 (2011) 7127–7138, https://doi.org/10.1016/j.biomaterials.2011.06.024.

[23] J. Mohanty, N. Thakur, S. Dutta Choudhury, N. Barooah, H. Pal, A.C. Bhasikuttan, Recognition-mediated light-up of thiazole orange with cucurbit[8]uril: exchange and release by chemical stimuli, J. Phys. Chem. B 116 (2012) 130–135, https://doi.org/10.1021/jp210432t.

[24] N.I. Shank, K.J. Zanotti, F. Lanni, P.B. Berget, B.A. Armitage, Enhanced photostability of genetically encodable fluoromodules based on fluorogenic cyanine dyes and a promiscuous protein partner, J. Am. Chem. Soc. 131 (2009) 12960–12969, https://doi.org/10.1021/ja9016864.

[25] E.E. Rastede, M. Tanha, D. Yaron, S.C. Watkins, A.S. Waggoner, B.A. Armitage, Spectral fine tuning of cyanine dyes: electron donor–acceptor substituted analogues of thiazole orange, Photochem. Photobiol. Sci. 14 (2015) 1703–1712, https://doi.org/10.1039/C5PP00117J.

[26] N.I. Shank, H.H. Pham, A.S. Waggoner, B.A. Armitage, Twisted Cyanines: A Non-Planar Fluorogenic Dye with Superior Photostability and its Use in a Protein-Based Fluoromodule, J. Am. Chem. Soc. 135 (2013) 242–251, https://doi.org/10.1021/ja308629w.

[27] A.A. Vasilev, M.I. Kandinska, S.S. Stoyanov, S.B. Yordanova, D. Sucunza, J.J. Vaquero, O.D. Castaño, S. Baluschev, S.E. Angelova, Halogen-containing thiazole orange analogues – new fluorogenic DNA stains, Beilstein J. Org. Chem. 13 (2017) 2902–2914, https://doi.org/10.3762/bjoc.13.283.

[28] A. Kurutos, O. Ryzhova, U. Tarabara, V. Trusova, G. Gorbenko, N. Gadjev,

T. Deligeorgiev, Novel synthetic approach to near-infrared heptamethine cyanine dyes and spectroscopic characterization in presence of biological molecules, J. Photochem. Photobiol. A: Chem. 328 (2016) 87–96, https://doi.org/10.1016/j.jphotochem.2016.05.019.
[29] A.A. Vasilev, M.I. Kandinska, S.S. Stoyanov, S.B. Yordanova, D. Sucunza, J.J. Vaquero, O.D. Castaño, S. Baluschev, S.E. Angelova, Halogen-containing thiazole orange analogues – new fluorogenic DNA stains, Beilstein J. Org. Chem. 13 (2017) 2902–2914, https://doi.org/10.3762/bjoc.13.283.
[30] A. Kurutos, I. Crnolatac, I. Orehovec, N. Gadjev, I. Piantanida, T. Deligeorgiev, Novel synthetic approach to asymmetric monocationic trimethine cyanine dyes derived from N-ethyl quinolinum moiety. Combined fluorescent and ICD probes for AT-DNA labelling, J. Luminescence. 174 (2016) 70–76, https://doi.org/10.1016/j.jlumin.2016.01.035.
[31] T. Deligeorgiev, A. Kurutos, N. Gadjev, 1-(3-Iodopropyl)-4-methylquinolin-1-ium iodide, Molbank 2015 (2015) M874, https://doi.org/10.3390/M874.
[32] P.R. Bohländer, T. Vilaivan, H.-A. Wagenknecht, Strand displacement and duplex invasion into double-stranded DNA by pyrrolidinyl peptide nucleic acids, Org. Biomol. Chem. 13 (2015) 9223–9230, https://doi.org/10.1039/C5OB01273B.
[33] A. Kurutos, O. Ryzhova, V. Trusova, G. Gorbenko, N. Gadjev, T. Deligeorgiev, Symmetric meso-chloro-Substituted pentamethine cyanine dyes containing Benzothiazolyl/Benzoselenazolyl chromophores novel synthetic approach and studies on photophysical properties upon interaction with bio-objects, J. Fluoresc. 26 (2016) 177–187, https://doi.org/10.1007/s10895-015-1700-4.
[34] I. Piantanida, B.S. Palm, P. Čudić, M. Žinić, H.-J. Schneider, Interactions of acyclic and cyclic bis-phenanthridinium derivatives with ss- and ds-polynucleotides, Tetrahedron. 60 (2004) 6225–6231, https://doi.org/10.1016/j.tet.2004.05.009.
[35] G. Scatchard, The attractions of proteins for small molecules and ions, Ann. N. Y. Acad. Sci. 51 (1949) 660–672, https://doi.org/10.1111/j.1749-6632.1949.tb27297.x.
[36] J.D. McGhee, P.H. von Hippel, Theoretical aspects of DNA-protein interactions: co-operative and non-co-operative binding of large ligands to a one-dimensional homogeneous lattice, J. Mol. Biol. 86 (1974) 469–489, https://doi.org/10.1016/0022-2836(74)90031-X.
[37] M.B. Hansen, S.E. Nielsen, K. Berg, Re-examination and further development of a precise and rapid dye method for measuring cell growth/cell kill, J. Immunol. Methods 119 (1989) 203–210, https://doi.org/10.1016/0022-1759(89)90397-9.
[38] T. Deligeorgiev, A. Vasilev, K.-H. Drexhage, Synthesis of novel cyanine dyes containing carbamoylethyl component – noncovalent labels for nucleic acids detection, Dye. Pigment. 74 (2007) 320–328, https://doi.org/10.1016/j.dyepig.2006.02.010.
[39] A. Vasilev, T. Deligeorgiev, N. Gadjev, K.-H. Drexhage, Synthesis of novel monomeric and homodimeric cyanine dyes based on oxazolo[4,5-b]pyridinium and quinolinium end groups for nucleic acid detection, Dye. Pigment. 66 (2005) 135–142, https://doi.org/10.1016/j.dyepig.2004.09.019.
[40] US6887668B2 - Nucleic Acid Separation and Detection by Electrophoresis With a Counter-Migrating High-Affinity Intercalating Dye, (2005).
[41] Larry A. Sklar, Flow Cytometry for Biotechnology, Oxford University Press, 2005.
[42] P. Alexander, Demchenko, Introduction to Fluorescence Sensing, Springer International Publishing, 2008.
[43] H. Zipper, H. Brunner, J. Bernhagen, F. Vitzthum, Investigations on DNA intercalation and surface binding by SYBR Green I, its structure determination and methodological implications, Nucleic Acids Res. 32 (2004) e103, https://doi.org/10.1093/nar/gnh101.
[44] R.B. Woodward, Structure and the absorption spectra of α,β-Unsaturated ketones, J. Am. Chem. Soc. 63 (1941) 1123–1126, https://doi.org/10.1021/ja01849a066.
[45] L.F. Fieser, M. Fieser, S. Rajagopalan, Absorption spectroscopy and the structures of the diosterols, J. Org. Chem. 13 (1948) 800–806, https://doi.org/10.1021/jo01164a003.
[46] J.R. Kanofsky, P.D. Sima, Structural and environmental requirements for quenching of singlet oxygen by cyanine dyes †, Photochem. Photobiol. 71 (2000) 361–368, https://doi.org/10.1562/0031-8655(2000)0710361SAERFQ2.0.CO2.
[47] J.T. Piechocki, K. Thoma, Pharmaceutical Photostability and Stabilization Technology, CRC Press, 2006.
[48] M. Quaranta, M. Murkovic, I. Klimant, A new method to measure oxygen solubility in organic solvents through optical oxygen sensing, Analyst. 138 (2013) 6243–6245, https://doi.org/10.1039/C3AN36782G.
[49] C.-H. Wu, J.-M. Chern, Kinetics of photocatalytic decomposition of methylene blue, Ind. Eng. Chem. Res. 45 (2006) 6450–6457, https://doi.org/10.1021/ie0602759.
[50] Gdel V. Morales, E.L. Sham, R. Cornejo, E.M. Farfan Torres, Kinetic Studies of the Photocatalytic Degradation of Tartrazine, (2012) http://ri.conicet.gov.ar/handle/11336/60800.
[51] X. Chen, X. Peng, A. Cui, B. Wang, L. Wang, R. Zhang, Photostabilities of novel heptamethine 3H-indolenine cyanine dyes with different N-substituents, J. Photochem. Photobiol. A: Chem. 181 (2006) 79–85, https://doi.org/10.1016/j.jphotochem.2005.11.004.
[52] B.R. Renikuntla, H.C. Rose, J. Eldo, A.S. Waggoner, B.A. Armitage, Improved photostability and fluorescence properties through polyfluorination of a cyanine dye, Org. Lett. 6 (2004) 909–912, https://doi.org/10.1021/ol036081w.
[53] N.M. Berezina, M.B. Berezin, A.S. Semeikin, Solvation interactions and photostability of tetrakis(1-methylpyridyl)porphyrin derivatives, J. Mol. Liq. 290 (2019) 111196, , https://doi.org/10.1016/j.molliq.2019.111196.
[54] I. Rosenthal, A. Frimer, The quenching effect of iodide ion on singlet oxygen, Photochem. Photobiol. 23 (1976) 209–211, https://doi.org/10.1111/j.1751-1097.1976.tb07244.x.
[55] F. Mandim, V.C. Graça, R.C. Calhelha, I.L.F. Machado, L.F.V. Ferreira, I.C.F.R. Ferreira, P.F. Santos, Synthesis, Photochemical and In Vitro Cytotoxic Evaluation of New Iodinated Aminosquaraines as Potential Sensitizers for Photodynamic Therapy, Molecules. 24 (2019) 863, https://doi.org/10.3390/molecules24050863.
[56] A. Gollmer, A. Felgenträger, W. Bäumler, T. Maisch, A. Späth, A novel set of symmetric methylene blue derivatives exhibits effective bacteria photokilling – a structure–response study, Photochem. Photobiol. Sci. 14 (2015) 335–351, https://doi.org/10.1039/C4PP00309H.
[57] S. Prodhomme, J.-P. Demaret, S. Vinogradov, U. Asseline, L. Morin-Allory, P. Vigny, A theoretical and experimental study of two thiazole orange derivatives with single- and double-stranded oligonucleotides, polydeoxyribonucleotides and DNA, J. Photochem. Photobiol. B, Biol. 53 (1999) 60–69, https://doi.org/10.1016/S1011-1344(99)00127-X.
[58] G.L. Silva, V. Ediz, D. Yaron, B.A. Armitage, Experimental and computational investigation of unsymmetrical cyanine dyes: understanding torsionally responsive fluorogenic dyes, J. Am. Chem. Soc. 129 (2007) 5710–5718, https://doi.org/10.1021/ja070025z.
[59] K. Vus, M. Girych, V. Trusova, G. Gorbenko, A. Kurutos, A. Vasilev, N. Gadjev, T. Deligeorgiev, Cyanine dyes derived inhibition of insulin fibrillization, J. Mol. Liq. 276 (2019) 541–552, https://doi.org/10.1016/j.molliq.2018.11.149.
[60] E.Y. Chernikova, S.V. Tkachenko, O.A. Fedorova, A.S. Peregudov, I.A. Godovikov, N.E. Shepel, S. Minkovska, A. Kurutos, N. Gadjev, T.G. Deligeorgiev, Y.V. Fedorov, Multistep assembling via intermolecular interaction between (bis)styryl dye and cucurbit[7]uril: spectral effects and host sliding motion, Dyes Pigm. 131 (2016) 206–214, https://doi.org/10.1016/j.dyepig.2016.04.013.
[61] K. Vus, U. Tarabara, A. Kurutos, O. Ryzhova, G. Gorbenko, V. Trusova, N. Gadjev, T. Deligeorgiev, Aggregation behavior of novel heptamethine cyanine dyes upon their binding to native and fibrillar lysozyme, Mol. Biosyst. 13 (2017) 970–980, https://doi.org/10.1039/C7MB00185A.
[62] M. Caprasse, C. Houssier, Do planar alkaloids from Strychnos usambarensis intercalate into the DNA helix? Biochimie. 65 (1983) 157–167, https://doi.org/10.1016/S0300-9084(83)80187-4.
[63] S. Aydinoglu, A. Pasti, T. Biver, B. Mennucci, Auramine O interaction with DNA: a combined spectroscopic and TD-DFT analysis, Phys. Chem. Chem. Phys. 21 (2019) 20606–20612, https://doi.org/10.1039/C9CP03071A.
[64] M. Deiana, Z. Pokladek, J. Olesiak-Banska, P. Młynarz, M. Samoc, K. Matczyszyn, Photochromic switching of the DNA helicity induced by azobenzene derivatives, Sci. Rep. 6 (2016) 1–8, https://doi.org/10.1038/srep28605.
[65] M. Sirajuddin, S. Ali, A. Badshah, Drug–DNA interactions and their study by UV–Visible, fluorescence spectroscopies and cyclic voltametry, J. Photochem. Photobiol. B, Biol. 124 (2013) 1–19, https://doi.org/10.1016/j.jphotobiol.2013.03.013.
[66] M. Deiana, K. Matczyszyn, J. Massin, J. Olesiak-Banska, C. Andraud, M. Samoc, Interactions of isophorone derivatives with DNA: spectroscopic studies, PLoS One 10 (2015) e0129817, , https://doi.org/10.1371/journal.pone.0129817.
[67] W. Saenger, Principles of Nucleic Acid Structure, Springer-Verlag, New York, 1984, https://doi.org/10.1007/978-1-4612-5190-3.
[68] A. Paul, P. Guo, D.W. Boykin, W.D. Wilson, A new generation of minor-groove-Binding—heterocyclic diamidines that recognize g·C base pairs in an AT sequence context, Molecules. 24 (2019) 946, https://doi.org/10.3390/molecules24050946.
[69] P. Peixoto, Y. Liu, S. Depauw, M.-P. Hildebrand, D.W. Boykin, C. Bailly, W.D. Wilson, M.-H. David-Cordonnier, Direct inhibition of the DNA-binding activity of POU transcription factors Pit-1 and Brn-3 by selective binding of a phenyl-furan-benzimidazole dication, Nucleic Acids Res. 36 (2008) 3341–3353, https://doi.org/10.1093/nar/gkn208.
[70] R. Nanjunda, W.D. Wilson, Binding to the DNA minor groove by heterocyclic dications: from AT-Specific monomers to GC recognition with dimers, Curr. Protoc. Nucleic Acid Chem. 51 (2012) 8.8.1–8.8.20, https://doi.org/10.1002/0471142700.nc0808s51.
[71] P. Majumder, D. Dasgupta, Effect of DNA groove binder distamycin a upon chromatin structure, PLoS One 6 (2011) e26486, , https://doi.org/10.1371/journal.pone.0026486.
[72] F. Han, N. Taulier, T.V. Chalikian, Association of the minor groove binding drug hoechst 33258 with d(CGCGAATTCGCG)2: volumetric, calorimetric, and spectroscopic characterizations, Biochemistry. 44 (2005) 9785–9794, https://doi.org/10.1021/bi047374f.
[73] H.J. Karlsson, M. Eriksson, E. Perzon, B. Åkerman, P. Lincoln, G. Westman, Groove-binding unsymmetrical cyanine dyes for staining of DNA: syntheses and characterization of the DNA-binding, Nucleic Acids Res. 31 (2003) 6227–6234, https://doi.org/10.1093/nar/gkg821.
[74] H.J. Karlsson, M.H. Bergqvist, P. Lincoln, G. Westman, Syntheses and DNA-binding studies of a series of unsymmetrical cyanine dyes: structural influence on the degree of minor groove binding to natural DNA, Bioorg. Med. Chem. 12 (2004) 2369–2384, https://doi.org/10.1016/j.bmc.2004.02.006.
[75] X. Wang, U.J. Krull, Tethered thiazole orange intercalating dye for development of fibre-optic nucleic acid biosensors, Anal. Chim. Acta 470 (2002) 57–70, https://doi.org/10.1016/S0003-2670(02)00671-2.
[76] H. Ihmels, K. Faulhaber, D. Vedaldi, F. Dall'Acqua, G. Viola, Intercalation of organic dye molecules into double-stranded DNA. Part 2: the annelated quinolizinium ion as a structural motif in DNA intercalators†, Photochem. Photobiol. 81 (2005) 1107–1115, https://doi.org/10.1562/2005-01-25-IR-427.
[77] J. Nygren, N. Svanvik, M. Kubista, The interactions between the fluorescent dye thiazole orange and DNA, Biopolymers. 46 (1998) 39–51, https://doi.org/10.1002/(SICI)1097-0282(199807)46:1<39::AID-BIP4>3.0.CO;2-Z.
[78] A. Kurutos, O. Ryzhova, V. Trusova, U. Tarabara, G. Gorbenko, N. Gadjev, T. Deligeorgiev, Novel asymmetric monomethine cyanine dyes derived from sulfobetaine benzothiazolium moiety as potential fluorescent dyes for non-covalent labeling of DNA, Dye. Pigment. 130 (2016) 122–128, https://doi.org/10.1016/j.

dyepig.2016.03.021.
[79] E. Yalçin, M. Matković, M. Jukić, L.G. Obrovac, I. Piantanida, Z. Seferoğlu, Novel fluorene/fluorenone DNA and RNA binders as efficient non-toxic ds-RNA selective fluorescent probes, Tetrahedron. 74 (2018) 535–543, https://doi.org/10.1016/j.tet.2017.12.008.
[80] S. Kaloyanova, I. Crnolatac, N. Lesev, I. Piantanida, T. Deligeorgiev, Synthesis and study of nucleic acids interactions of novel monomethine cyanine dyes, Dye. Pigment. 92 (2012) 1184–1191, https://doi.org/10.1016/j.dyepig.2011.08.019.
[81] M. Dukši, D. Baretić, V. Čaplar, I. Piantanida, Novel bis-phenanthridine derivatives with easily tunable linkers, study of their interactions with DNA and screening of antiproliferative activity, Eur. J. Med. Chem. 45 (2010) 2671–2676, https://doi.org/10.1016/j.ejmech.2010.02.017.
[82] E. Jastrzębska, U. Bazylińska, M. Bułka, K. Tokarska, M. Chudy, A. Dybko, K.A. Wilk, Z. Brzózka, Microfluidic platform for photodynamic therapy cytotoxicity analysis of nanoencapsulated indocyanine-type photosensitizers, Biomicrofluidics. 10 (2016) 014116, , https://doi.org/10.1063/1.4941681.
[83] I.S.-R. Vaisertrager, O.I. Podgornaya, N.I. Enukashvily, Constitutive heterochromatin DNA fragments are demethylated and decondensed in senescent primary fibroblasts MRC5 and malignant A431 cell line, Cell Tiss. Biol. 1 (2007) 50–57, https://doi.org/10.1134/S1990519X07010075.
[84] S. Khamchun, V. Thongboonkerd, Cell cycle shift from G0/G1 to S and G2/M phases is responsible for increased adhesion of calcium oxalate crystals on repairing renal tubular cells at injured site, Cell Death Discov. 4 (2018) 1–12, https://doi.org/10.1038/s41420-018-0123-9.
[85] H.M. Davey, Flow cytometric techniques for the detection of microorganisms, Methods Cell Sci. 24 (2002) 91–97, https://doi.org/10.1023/A:1024106317540.
[86] B. Buysschaert, L. Vermijs, A. Naka, N. Boon, B.D. Gusseme, Online flow cytometric monitoring of microbial water quality in a full-scale water treatment plant, Npj Clean Water 1 (2018) 1–7, https://doi.org/10.1038/s41545-018-0017-7.
[87] S. Müller, G. Nebe-von-Caron, Functional single-cell analyses: flow cytometry and cell sorting of microbial populations and communities, FEMS Microbiol. Rev. 34 (2010) 554–587, https://doi.org/10.1111/j.1574-6976.2010.00214.x.
[88] M. Vignola, D. Werner, F. Hammes, L.C. King, R.J. Davenport, Flow-cytometric quantification of microbial cells on sand from water biofilters, Water Res. 143 (2018) 66–76, https://doi.org/10.1016/j.watres.2018.05.053.